Eur. Phys. J. B **9**, 545–549 (1999)

THE EUROPEAN PHYSICAL JOURNAL B

EDP Sciences

Characterization of a large vortex using acoustic time-reversal mirrors

S. Manneville[1,a], A. Maurel[1,2], P. Roux[1], and M. Fink[1]

[1] Laboratoire Ondes et Acoustique[b], ESPCI, Université Paris VII, 10 rue Vauquelin, 75005 Paris, France
[2] Laboratoire de Physique et Mécanique des Milieux Hétérogènes[c], ESPCI, 10 rue Vauquelin, 75005 Paris, France

Received 23 April 1998

Abstract. We report new results on the ultrasonic characterization of a fluid flow using an acoustic time-reversal mirror (TRM). The structure of a large vortex generated by a rotating disk in a hollow cylinder is investigated both inside and below the cylinder. For mean-flow characterization, the TRM is shown to be a powerful vorticity detector. Experimental time-of-flight data are successfully compared to a numerical simulation of the flow and the orthoradial velocity is reconstructed using simple geometrical acoustics. Real-time measurements allow us to extract the precession motion of the vortex, providing direct, non-intrusive, and dynamical information on the flow.

PACS. 43.30+m Underwater sound – 43.35+d Ultrasonics, quantum acoustics, and physical effects of sound – 47.32-y Rotational flow and vorticity

1 Introduction

Acoustic waves provide a direct, non-intrusive and non-localized way of probing hydrodynamic flow fields and several approaches have been proposed in the literature *e.g.* ultrasound scattering [1–5] or acoustic tomography [6–9]. In a previous work, we used a time-reversal mirror (TRM) [10] to show that vorticity breaks time-reversal invariance for acoustic waves [11]. We also studied the interaction of a plane incident wave with two different flows (a large vortex and a vorticity filament) showing that a double TRM acts as an artificial vorticity amplifier and allows a global characterization of a vortex [12]. In this paper, we first describe the experimental set-up and method. Then we focus on the quantitative characterization of the mean flow in a Von Kármán-like geometry [13,14], and present both a simulation and a reconstruction of the orthoradial fluid velocity. Eventually we turn to a real-time investigation of the vortex.

2 Experimental set-up and method

2.1 Experimental set-up

The flow field under investigation is generated by a disk of diameter $d = 60$ mm rotating at the top of a hollow, open Plexiglas cylinder (inner diameter 75 mm, outer diameter 80 mm) at a frequency $\Omega_\mathrm{d}/2\pi \simeq$ 1-10 Hz, which yields a Reynolds number $\mathrm{Re} = \Omega_\mathrm{d} d^2/4\nu \simeq 10^3$-$10^4$. The disk is fitted with four blades (10 mm high) to enhance the rotation in the fluid. The cylinder is 240 mm long and immersed in a large water container (see Fig. 1). The double TRM consists of two piezoelectric transducer arrays placed in front of each other, on either side of the flow at a distance $D \simeq 100$ mm. Each array (TRM1 and TRM2) is made of 64 transducers, with a spacing of 0.42 mm and works at a central frequency of $\omega/2\pi = 3.5$ MHz with a sampling frequency of 20 MHz. Such a set-up enables us to scan the flow field spatially by moving around the double TRM.

2.2 Spatial and temporal resolutions

The effects of fluid motion on an acoustic wave are both spatial and temporal [15]. Indeed, due to velocity gradients, acoustic rays are refracted and for low Mach numbers M, $\mathrm{d}\mathbf{n}/\mathrm{d}t = (\nabla \times \mathbf{u}) \times \mathbf{n}$, where $\mathbf{n}$ is the unit vector along the direction of propagation and $\mathbf{u}(\mathbf{r})$ is the fluid velocity field. For an acoustic ray propagating over a distance D, this yields a spatial deflection $\delta x \sim MD$. In our experiment, the characteristic fluid velocity is $u \simeq 10$ cm/s and the sound speed $c \simeq 1500$ m/s so that $M = u/c \simeq 10^{-4}$. With $D \simeq 100$ mm, one gets $\delta x \simeq 10^{-2}$ mm. Since the spatial resolution is given by the array pitch 0.42 mm, we may neglect refraction and assume a straight-ray propagation.

Fluid motion also results in a local modification of the scalar speed of sound according to $c(\mathbf{r}) = c + \mathbf{u}(\mathbf{r}) \cdot \mathbf{n}$. For

[a] e-mail: `sebastien.manneville@espci.fr`
[b] URA CNRS 1503
[c] URA CNRS 857

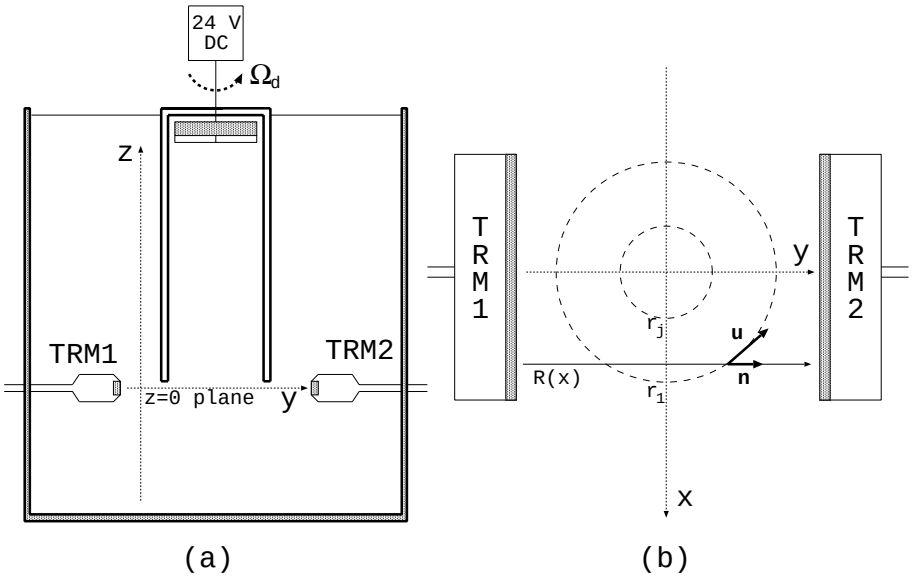

Fig. 1. Experimental set-up. (a) Front view. (b) Top view in the plane $z = 0$.

a vortex of characteristic size $L \simeq 100$ mm, this leads to a time shift $\delta t \sim ML/c \simeq 10^{-8}$ s of the acoustic signal (*i.e.* to a phase shift $\delta\phi \sim \omega ML/c \simeq 0.2$ rad). Experimentally, time shifts are inferred from Fourier transforms of the acoustic signals and the temporal resolution is fixed by the electronic noise level ($\delta t \simeq 10^{-9}$ s), which allows a good detection of fluid velocities down to about 2 cm/s. Note that this analysis based on geometrical acoustics assumes that the vortex is "large" *i.e.* that L is much larger than the acoustic wavelength $\lambda \simeq 0.5$ mm. When $L \simeq \lambda$, scattering by the vortex core has to be taken into account [1–5,12].

2.3 Experimental method

The experimental measurements are performed as follows. First, two plane waves are simultaneously emitted by the two TRMs and received after one crossing of the flow. This yields the direct (*e.g.* from TRM1 to TRM2) and inverse (from TRM2 to TRM1) times-of-flight $t_{1\to2}$ and $t_{2\to1}$ across the vorticity field as a function of the transducer position x. The acoustic signals are then time-reversed and simultaneously reemitted by the two TRMs, so that the time-reversal procedure can be further iterated.

In the absence of fluid motion, the acoustic wave is supposed to remain plane after several trips between the TRMs. However, due to the finite aperture of the transducer arrays, the wavefronts are distorted by diffraction effects [16]. We were thus led to perform a first "blank" experiment in order to measure the times-of-flight $t^{(0)}_{1\to2}$ and $t^{(0)}_{2\to1}$ in the absence of fluid flow. Those references $t^{(0)}_{1\to2}$ and $t^{(0)}_{2\to1}$ are then subtracted to $t_{1\to2}$ and $t_{2\to1}$ measured in the presence of a vortex, yielding the direct and inverse time shifts $\delta t_{1\to2}$ and $\delta t_{2\to1}$.

Such time shifts not only account for fluid motion effects but also for possible effects of temperature or density inhomogeneities on the local sound speed. To focus on the fluid motion effects only, we compute the phase distortion $\Delta\phi(x) = (\phi_{1\to2}(x) - \phi_{2\to1}(x))/2$, where $\phi_{1\to2} = \omega\delta t_{1\to2}$ and $\phi_{2\to1} = \omega\delta t_{2\to1}$ [8,9]. After one crossing of the velocity field $\mathbf{u}(\mathbf{r})$, a straightforward calculation to first order in M yields

$$\Delta\phi(x) = -\frac{\omega}{c^2}\int_{R(x)} \mathbf{u}\cdot\mathbf{n}\,\mathrm{d}s, \qquad (1)$$

where s is the position along the acoustic ray $R(x)$ (see Fig. 1). After N crossings of the flow *i.e.* after $N-1$ time-reversal processes, the phase distortion is given by $\Delta\phi_N(x) = N\Delta\phi(x)$ [12,16], so that the double TRM can be seen as a (linear) vorticity amplifier which allows the detection of small flow velocities (down to about 3 mm/s for $N = 7$). Note, however, that refraction as well as diffraction effects are also amplified by iterative time-reversal processes (*e.g.* for the spatial deflection of an acoustic ray, $\delta x_N = N\delta x$ after N crossings of the flow [11]). In the present configuration, such effects were experimentally estimated to remain negligible as long as $N < 13$.

3 Study of the mean flow below the cylinder ($z \leq 0$)

3.1 The double TRM as a vorticity amplifier

Figure 2a shows the mean phase distortions $\Delta\phi_1(x)$, $\Delta\phi_4(x)$, and $\Delta\phi_{10}(x)$ in the plane $z = 0$ and averaged over 200 measurements on the same vortex. The error bars correspond to the standard deviation of the phase signals measured in the absence of fluid motion: typically, $(\Delta\phi_N(x))_{\text{r.m.s.}} \simeq 0.005\sqrt{N}$ rad. As expected, the effect of vorticity on acoustic propagation is amplified

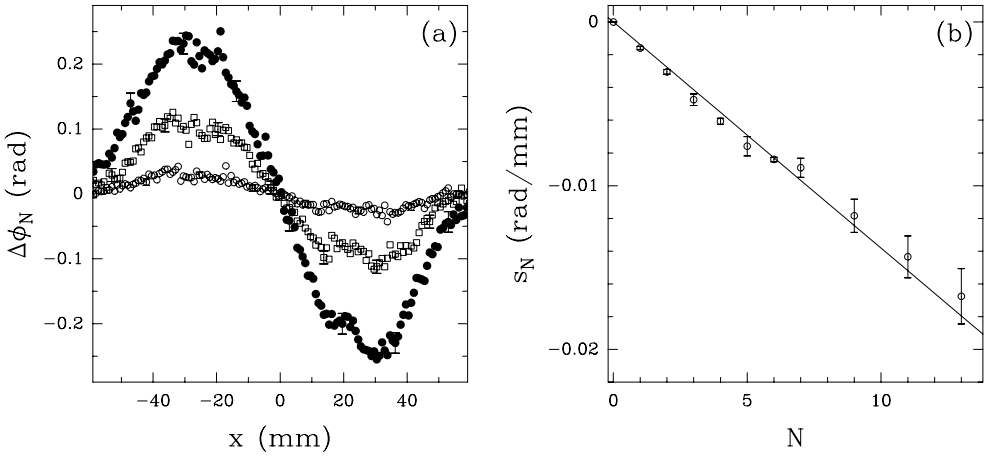

Fig. 2. (a) Phase distortions $\Delta\phi_N(x)$ measured in the plane $z = 0$ for $\Omega_d/2\pi = 3.2$ Hz and $N = 1$ (○), $N = 4$ (□), and $N = 10$ (●). (b) Slope $s_N = \mathrm{d}(\Delta\phi_N)/\mathrm{d}x$ for $x = 0$ as a function of the number of crossings N in the plane $z = 0$ (○). Such phase distortions were obtained with five displacements of the TRMs. The errorbars account for the standard deviation of s_N when varying the range for linear interpolation of $\Delta\phi_N$ around $x = 0$. The straight line is $s_N = -2N\Omega\omega R/c^2$ with $R = 43$ mm and $\Omega/2\pi = 0.25$ Hz.

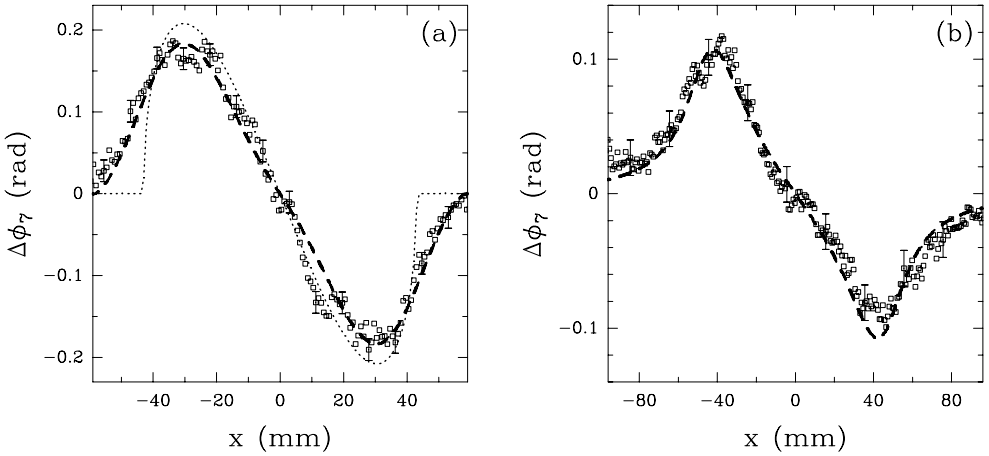

Fig. 3. (a) Phase distortion after 7 crossings of the flow measured in the plane $z = 0$ (□), theoretical prediction of the solid body rotation with $R = 43$ mm and $\Omega/2\pi = 0.25$ Hz (dotted line), and simulated phase distortion computed from the FLUENT velocity field (thick dashed line). (b) Phase distortion after 7 crossings of the flow measured in the plane $z = -40$ mm (□) and simulated phase distortion computed from the FLUENT velocity field (thick dashed line). Both experimental phase distortions were obtained for $\Omega_d/2\pi = 3.2$ Hz. The orthoradial velocities from the FLUENT simulation are shown in Figure 4.

by the time-reversal process. To check the linearity of the amplification, we plotted the slope s_N of $\Delta\phi_N(x)$ at the center of the vortex (*i.e.* at the position where $\Delta\phi = 0$, which is taken to be $x = 0$ by convention) *versus* N (fig. 2(b)). Linearity remains very good up to more than 10 time-reversal processes.

As mentioned in reference [12], a solid body rotation of radius R and frequency $\Omega/2\pi$ yields $\Delta\phi_N(x) = -2N\Omega\omega x\sqrt{R^2 - x^2}/c^2$. This analytical shape provides rather good estimates of $R = 43$ mm $\pm 5\%$ and $\Omega/2\pi = 0.25$ Hz $\pm 5\%$ for a driving frequency $\Omega_d/2\pi = 3.2$ Hz (see Fig. 3a). These estimates are also in quantitative agreement with the linear predicted behaviour of s_N *vs.* N: $s_N = -2N\Omega\omega R/c^2$. Using the amplification property, this method allowed us to detect rotations as slow as 0.05 Hz.

3.2 Simulation and reconstruction of the orthoradial component of the velocity

As seen in Figure 3a, deviations from the solid rotation prediction show up for large values of $|x|$ *i.e.* on the edges of the vortex. Indeed, below the cylinder, the flow is unbounded so that a discontinuity of the fluid orthoradial velocity from $u_\theta(r = R, z) = R\Omega$ to zero for $r > R$ is not physical. To get a qualitative picture of the structure of the mean flow, we used the FLUENT code, based on a finite volume method, to simulate an incompressible and

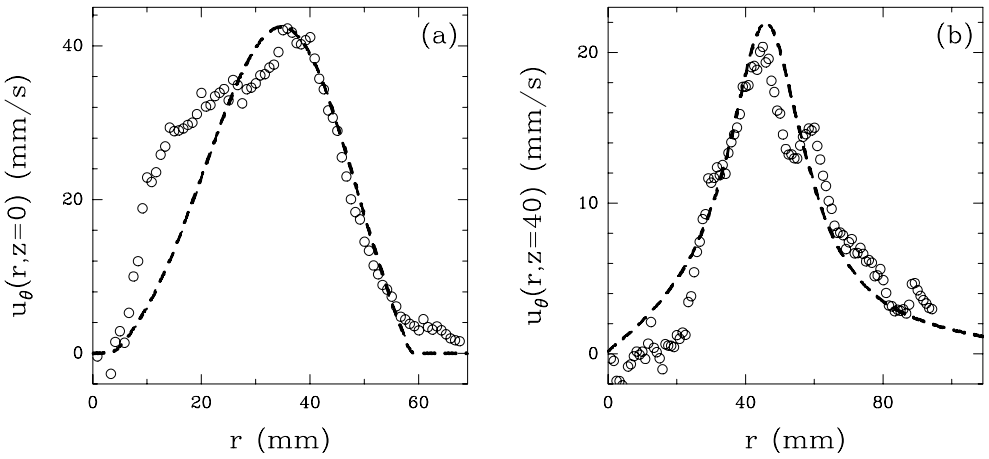

Fig. 4. Orthoradial component of the velocity: reconstructed from $\Delta\phi_7(x)$ using the algorithm described in the text (○) and simulated by the FLUENT code in a configuration close to the experimental one (thick dashed line). (a) $z = 0$. (b) $z = -40$ mm.

axisymmetric flow in a geometry as close to the experimental one as possible (blades, for instance, were not taken into account but one may assume that far from the rotating disk, the mean velocity fields show the same features). In such an axisymmetric geometry, the contribution of the radial velocity $u_r(r, z)$ to the integral in equation (1) is easily proven to be always zero, so that for a given value of z, $\Delta\phi(x)$ depends only on the orthoradial velocity $u_\theta(r, z)$. The orthoradial velocity given by the simulation was rescaled both in space and amplitude and used for computing the phase distortion through equation (1). As reported in Figure 3a, for $z = 0$, the phase distortion computed from the simulated velocity field yields a better approximation of the experimental data than the solid rotation assumption around the edges of the vortex. This gets more obvious as one goes deeper below the cylinder: for $z = -40$ mm, the flow can no longer be compared to a solid rotation, whereas the corresponding simulated phase distortion gives a good fit of the experimental one, except for small values of r. These differences may be attributed to the fact that in the numerical simulation, we could not achieve such high driving frequencies Ω_d as in the experiment nor take into account the presence of blades. Moreover, the simulation was run in an axisymmetric, laminar regime, whereas the experimental flow displays a precession motion, as shown in the next section.

Finally, to try and solve the inverse problem for $u_\theta(r, z)$, we built a simple reconstruction algorithm assuming that the flow is axisymmetric. The rotational zone is divided into p small concentric rings $r \in [r_{j+1}, r_j]$ where $u_\theta(r, z)$ is assumed to take some constant value u_j. r_1 is the edge of the vortex, r_{p+1} the center, and $p+2$ the number of experimental data points (see Fig. 1). The phase distortion $\varphi_i = \Delta\phi(x_{i+1})$ sampled at the transducer position x_{i+1} can then be computed through a discretized version of equation (1). Indeed, equation (1) turns into a linear system $\varphi_i = \mathcal{M}_{i,j}\, u_j$, where $\mathcal{M}_{i,j}$ accounts for the propagation of the acoustic ray $R(x_{i+1})$ inside the jth ring:

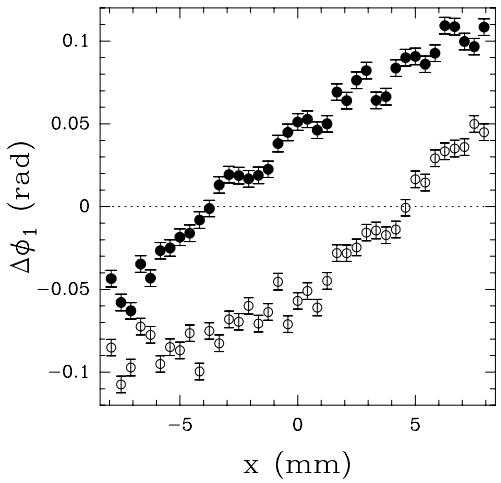

Fig. 5. Phase distortion measurements inside the cylinder with $\Omega_d/2\pi = 2.8$ Hz and $z = 90$ mm at times $t_1 = 0.71$ s (○) and $t_2 = 0.98$ s (●).

$$\mathcal{M}_{i,j} = -2\frac{\omega}{c^2}\int_{y_{i,j+1}}^{y_{i,j}} \cos(\mathbf{u},\mathbf{n})\,\mathrm{d}y = -2\frac{\omega}{c^2} r_{i+1} \ln\left[\frac{y_{i,j}+r_j}{y_{i,j+1}+r_{j+1}}\right] \text{ for } i \geq j, \qquad (2)$$

where $y_{i,j} = \sqrt{r_j^2 - r_{i+1}^2}$. Since $\mathcal{M}$ is an invertible, triangular matrix, u_j is easily reconstructed from the experimental values of φ_i. To achieve a good reconstruction, however, the experimental phase data had to be smoothed by averaging φ_i over its four nearest neighbours. The results are shown in Figure 4 for $z = 0$ and $z = -40$ mm, together with the simulated orthoradial velocity used in Figure 3. The agreement between the reconstruction and the simulation is good. Differences for small values of r, already noted in the phase distortion, also arise in the reconstructed velocity profiles for the same reasons.

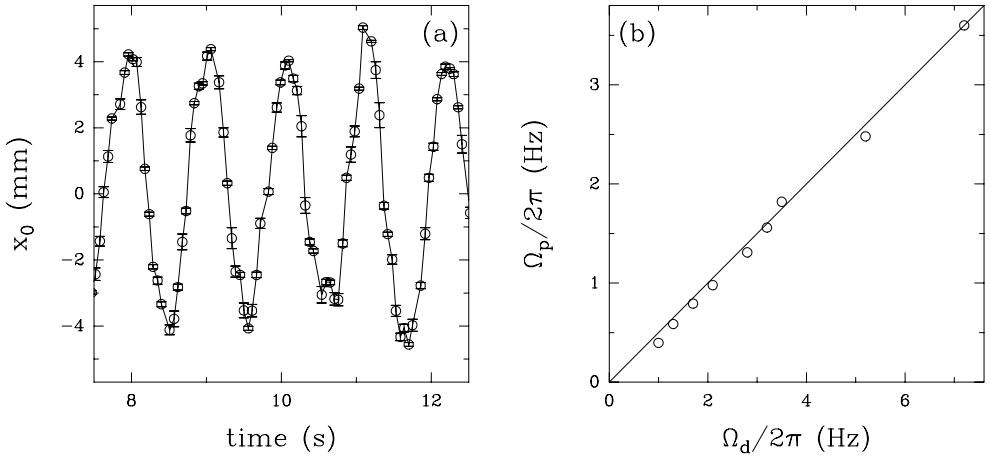

Fig. 6. Precession motion of the vortex inside the cylinder. (a) Position of the center of the vortex x_0 as a function of time ($\circ$ and solid line) with $\Omega_d/2\pi = 2.1$ Hz and $z = 90$ mm. (b) Precession frequency $\Omega_p/2\pi$ *vs.* driving frequency $\Omega_d/2\pi$ at $z = 90$ mm ($\circ$). The straight line is $\Omega_p/2\pi = 0.5\Omega_d/2\pi$.

4 Real-time tracking of the vortex inside the cylinder (z > 0)

Measurements of $\Delta\phi(x)$ were also performed at a sampling frequency of 15 Hz inside the cylinder where the flow is strong enough to allow a fast detection without time-reversal (flow velocities larger than 2 cm/s). Due to refraction at the water-Plexiglas interface, such measurements had to be restricted to the range $|x| < 8$ mm. Figure 5 shows that $\Delta\phi(x)$ is time-dependent *i.e.* that the vortex is not stationary, and we tracked the abscissa $x_0(t)$ of the center of the vortex (for which $\Delta\phi(x_0) = 0$) as a function of time. As seen in Figure 6a, the vortex undergoes a precession motion: x_0 oscillates with a frequency $\Omega_p/2\pi$ that was estimated by Fourier transforming $x_0(t)$ over a total recording time of about 35 s. Figure 6b shows that the precession frequency is very close to half the driving frequency for $\Omega_d/2\pi \simeq 1-7$ Hz. By moving the double TRM along the z-axis, for a given driving frequency, the precession frequency was shown to remain constant whereas the radius of the precession decreases with z (from 7 mm for $z = 50$ mm to 4 mm for $z = 90$ mm). Such features of the vortex precession are in qualitative agreement with previous observations on Von Kármán flows in slightly different experiments [14,17]. Moreover, in a closed configuration with two co-rotating disks, Pinton *et al.* [18] observed a precession motion at $\Omega_p \simeq 0.5(\Omega_1 + \Omega_2)$, where Ω_1 and Ω_2 are the rotation frequencies of the disks, which is consistent with our results when taking $\Omega_1 = \Omega_d$ and $\Omega_2 = 0$ *i.e.* when only one of the two disks is rotating.

5 Conclusions and perspectives

From the above results, the double TRM turns out to be a powerful tool for the investigation of hydrodynamic flows, both through its ability to amplify very small vorticity fields and through its real-time possibilities. This set-up also enabled us to achieve an accurate reconstruction of the orthoradial component of the velocity. Time-reversal experiments on more complex, unstationary flows and efforts to perform faster measurements and 2D tomography of fluid flows using circular transducer arrays are currently under progress in our laboratory.

The authors are very grateful to J.-L. Aider, Y. Couder, N. Mordant, J.-F. Pinton, C. Prada, J.-L. Thomas, and J. de Rosny for fruitful discussions.

References

1. P.R. Gromov, A.B. Ezerski, A.L. Fabrikant, Sov. Phys. Acoust. **28**, 552 (1982).
2. A.L. Fabrikant, Sov. Phys. Acoust. **29**, 152 (1983).
3. F. Lund, C. Rojas, Physica D **37**, 508 (1989).
4. C. Baudet, S. Ciliberto, J.-F. Pinton, Phys. Rev. Lett. **67**, 193 (1991).
5. P.V. Sakov, Sov. Phys. Acoust. **39**, 280 (1993).
6. D.W. Schmidt, P.M. Tilman, J. Acoust. Soc. Am. **47**, 1310 (1970).
7. R.H. Engler, D.W. Schmidt, W.J. Wagner, J. Acoust. Soc. Am. **85**, 72 (1989).
8. K.B. Winters, D. Rousseff, IEEE Ultrason. Ferroelec. Freq. Control **40**, 26 (1993).
9. S.A. Johnson, J.F. Greenleaf, M. Tanaka, G. Flandro, ISA Trans. **16**, 3 (1997).
10. M. Fink M., Phys. Today **50**, 34 (1997).
11. P. Roux, M. Fink, Europhys. Lett. **32**, 25 (1995).
12. P. Roux, M. Fink, Phys. Rev. Lett. **79**, 3170 (1997).
13. T. Von Kármán, Z. Angew. Math. Mech. **1**, 235 (1921).
14. R. Labbé, J.-F. Pinton, S. Fauve, Phys. Fluids **8**, 914 (1996).
15. L.D. Landau, E.M. Lifshitz, *Fluid Mechanics*, 2nd edn. (MIR, Moscow, 1989), Chap. 8.
16. P. Roux P., Ph. D. thesis, University of Paris VII (1997).
17. M. Piva, A. Calvo, J.E. Wesfreid, preprint (1999).
18. J.-F. Pinton, F. Chillà, N. Mordant, Eur. J. Mech. B **17**, 535-547 (1998).